

Clogging, Diode and Collective Effects of Skyrmions in Funnel Geometries

J. C. Bellizotti Souza¹, N. P. Vizarim², C. J. O. Reichhardt³, C. Reichhardt³ and P. A. Venegas¹

¹ Departamento de Física, Faculdade de Ciências, Unesp-Universidade Estadual Paulista, CP 473, 17033-360 Bauru, SP, Brazil

² POSMAT - Programa de Pós-Graduação em Ciência e Tecnologia de Materiais, Faculdade de Ciências, Universidade Estadual Paulista - UNESP, Bauru, SP, CP 473, 17033-360, Brazil

³ Theoretical Division and Center for Nonlinear Studies, Los Alamos National Laboratory, Los Alamos, New Mexico 87545, USA

E-mail: cjrx@lanl.gov, nicolas.vizarim@unesp.br

Abstract. Using a particle-based model, we examine the collective dynamics of skyrmions interacting with a funnel potential under dc driving as the skyrmion density and relative strength of the Magnus and damping terms are varied. For driving in the easy direction, we find that increasing the skyrmion density reduces the average skyrmion velocity due to jamming of skyrmions near the funnel opening, while the Magnus force causes skyrmions to accumulate on one side of the funnel array. For driving in the hard direction, there is a critical skyrmion density below which the skyrmions become trapped. Above this critical value, a clogging effect appears with multiple depinning and repinning states where the skyrmions can rearrange into different clogged configurations, while at higher drives, the velocity-force curves become continuous. When skyrmions pile up near the funnel opening, the effective size of the opening is reduced and the passage of other skyrmions is blocked by the repulsive skyrmion-skyrmion interactions. We observe a strong diode effect in which the critical depinning force is higher and the velocity response is smaller for hard direction driving. As the ratio of Magnus force to dissipative term is varied, the skyrmion velocity varies in a non-linear and non-monotonic way due to the pile up of skyrmions on one side of the funnels. At high Magnus forces, the clogging effect for hard direction driving is diminished.

1. Introduction

The dynamical behavior of vortices in superconductors, Wigner crystals, and colloidal particles subjected to confined geometries such as one-dimensional (1D) channels or constrictions [1, 2, 3], bottlenecks [4, 5, 6, 7], or asymmetric funnel walls [8, 9, 10, 11, 12] has been extensively investigated in the past years. In such systems, it is possible for a portion of the particles to become pinned by the confining walls, thereby hindering the motion of other particles due to the particle-particle interactions. Clogging is a generic phenomenon that has been studied for particles with contact interactions such as granular matter both with and without friction flowing through an aperture or orifice, where when the density is high enough, the flow can stop [13, 14, 15, 16, 17]. The clogging is probabilistic, and the system can flow for some time until the particles reach a certain configuration that stops the flow.

For systems of particles interacting with funnel arrays, there have been a variety of studies describing diode, ratchet, clogging and jamming effects for superconducting vortices [10, 18, 19, 11, 8, 20, 21], colloidal particles [22], and active matter [23, 24, 25]. In the case of superconducting vortices and colloids, the interactions are longer range compared to the contact forces found in granular matter. A periodic array of funnels can also produce commensurability effects in which the depinning threshold is significantly increased when the number of particles is an integer multiple of the number of plaquettes in the system [19, 10, 22]. Due to the asymmetry of the funnel geometry, the depinning and dynamics depend strongly on whether the drive is applied along the easy or hard direction of motion through the funnel. For driving in the easy direction, the velocity-force curves are generally smooth, while for driving in the hard direction, clogging dynamics can occur when particles accumulate along the funnel edges and block the flow.

Recently, a particle-based model of magnetic skyrmions was investigated in the presence of funnel geometries [26, 27]. Here a single skyrmion was subjected to ac driving, and it was possible to achieve precise control of the skyrmion motion through a ratchet effect [27]. The ratcheting can be induced with ac driving in the particle-based model, but could be produced by an oscillating field that changes the size of the skyrmion in a continuum model [26]. In the present work we examine collective behaviors including diode and jamming effects for assemblies of skyrmions interacting with a linear array of asymmetric funnels.

Skyrmions are spin textures wrapping a sphere pointing in all directions to form a topologically stable particle-like object [28, 29, 30] that can be set into motion by the application of a spin polarized current [31, 32, 33]. In the presence of external drives, skyrmions can show a depinning threshold similar to that found for superconducting vortices. The key difference between skyrmions and other overdamped particles is the presence of the Magnus force [34, 35]. This non-dissipative force produces a skyrmion velocity contribution that is perpendicular to the external applied current. In the case of a clean sample without defects, the skyrmions move at an angle with respect to the transport force known as the skyrmion Hall angle, θ_{sk}^{int} [34, 29, 36]. Experimentally, the skyrmion Hall angle ranges from a few degrees up to values very close to 90° depending on the system parameters [36, 37].

Recent advances in creating nanoengineered materials, where defects of different sizes and shapes can be embedded in a sample, permit the creation of complex structures that can interact with and guide skyrmions inside the material. In this work we use a particle-based simulation to describe the dynamical behavior of multiple skyrmions interacting with a linear array of asymmetric funnels under the influence of a dc drive. In previous works investigating single skyrmion dynamics under the influence of periodic and asymmetric potentials, we showed that the Magnus term can

significantly influence the dynamics and can produce quantized directions of motion [38, 39, 40], novel ratchet effects [41, 42, 27, 43, 44] and possibilities for controlled skyrmion motion [45]. When multiple interacting skyrmions are present in a sample, the skyrmion-skyrmion interactions can compete with the effects of the Magnus force. It was shown that in the presence of random disorder, an assembly of skyrmions flows in riverlike channels with individual skyrmions switching between pinned and moving states [46, 47], while for multiple skyrmions in periodic pinning, moving segregated states appear with clustering that arises due to the velocity dependence of the skyrmion Hall angle in the presence of strong pinning [48].

In this work, we investigate the collective interactions of skyrmions in a linear array of asymmetric funnels where a dc transport force is applied along the easy or hard direction. At low skyrmion density, for driving along the easy axis the dynamics is similar to that found in the single skyrmion case, where the average velocity increases linearly with increasing drive. As the skyrmion density increases, collective effects emerge and the skyrmions show a jamming effect near the funnel opening associated with a reduction in the average skyrmion velocity. For drives applied along the hard direction, below a critical skyrmion density there is no net skyrmion motion, while at higher densities the skyrmions can exhibit more than one finite depinning threshold due to reentrant pinning phases (RPPs) produced by clogging effects. In the RPPs, the skyrmion motion is interrupted due to a pile up of skyrmions inside funnel plaquettes, leading to formation of a clogged state where the skyrmions cannot move until a second depinning threshold is reached that opens the flow of skyrmions through the funnels once again. The clogging effect is probabilistic in nature, as indicated by the fact that the depinning and reentrant pinning transitions fall at different driving forces for different realizations. At higher drives, the velocity-force curves become continuous, and we map the transition from clogging behavior to continuous flow as a function of skyrmion density and driving force. A skyrmion diode effect is produced by the different responses of the driven skyrmions under different driving directions. We have also studied the effect of varying the ratio of the Magnus term to the dissipative term for both directions of driving, and find both non-linear and non-monotonic behavior. For hard direction driving, increasing the Magnus term can diminish and destroy the RPPs by reducing the tendency of the skyrmions to clog.

2. Simulation

We simulate the collective effects of skyrmions under the influence of a linear array of funnel potentials aligned along the x direction, as shown in Fig. 1. The simulation box has dimensions $L_x \times L_y$ with periodic boundary conditions in the x direction.

The skyrmions interact with each other, with the repulsive barrier walls that form the funnel geometry, and with an applied dc drive. The skyrmion dynamics is governed by equation (1) [49]:

$$\alpha_d \mathbf{v}_i + \alpha_m \hat{\mathbf{z}} \times \mathbf{v}_i = \mathbf{F}_i^{ss} + \mathbf{F}_W + \mathbf{F}^D \quad (1)$$

Here, \mathbf{v}_i is the velocity of the i th skyrmion. The first term on the left is the damping term that arises from the spin precession and dissipation of electrons in the skyrmion core, where α_d is the damping constant. The second term is the Magnus term produced by gyroscopic effects, where α_m is the Magnus constant. Throughout this work we use the normalization $\alpha_d^2 + \alpha_m^2 = 1.0$.

On the right side of equation (1), the first term is the repulsive skyrmion-skyrmion force given by the expression $\mathbf{F}^{ss} = \sum_i^N K_1(r_{ij}/\xi) \hat{\mathbf{r}}_{ij}$, where ξ is the screening length which we take to be 1.0 in dimensionless units, $r_{ij} = |\mathbf{r}_i - \mathbf{r}_j|$ is the distance between skyrmions i and j , and the unit vector $\hat{\mathbf{r}}_{ij} = (\mathbf{r}_i - \mathbf{r}_j)/r_{ij}$. For computational efficiency, we cut off the interaction beyond $r_{ij} = 6.0$ where

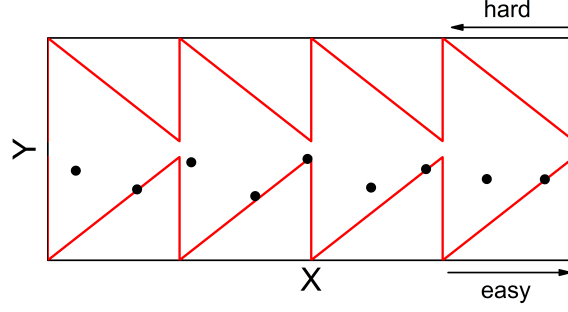


Figure 1. Illustration of the linear array of funnel potentials used in this work. Red lines are the repulsive barrier walls of the funnel geometry and black dots are skyrmions that are subjected to both damping and Magnus terms as well as a dc drive applied along the $+x$ or $-x$ direction. The hard and easy directions of motion are labeled with arrows.

the Bessel interaction becomes negligible. The sample size is fixed to $L_x = 35\xi$ and $L_y = 14\xi$. The second term on the right side is the funnel wall potential, which is modeled using a Gaussian function given by $U_W = U_0 e^{-r_{iw}^2/a_0^2}$, where U_0 is the potential strength, r_{iw} is the distance between the skyrmion i and the wall, and a_0 is the funnel wall thickness. The repulsive force exerted by the wall is $\mathbf{F}_W = -\nabla U_W$, giving $\mathbf{F}_W = F_0 r_{iw} e^{-r_{iw}^2/a_0^2} \hat{\mathbf{r}}_{iw}$ where $F_0 = 2U_0/a_0^2$. For this work we fix $a_0 = 0.02\xi$ and $U_0 = 1.0$. The number of funnels is fixed at $N_F = 4$ and the funnel opening is set to $O = 1.0\xi$. The skyrmion density is given by $\rho_{sk} = N_{sk}/L_x L_y$, where N_{sk} is the number of skyrmions in the sample. This quantity is normalized in terms of $1/\xi^2$.

The last term on the right side of equation (1) is the transport dc driving force $\mathbf{F}^D = F^D \hat{\mathbf{d}}$ with $\hat{\mathbf{d}} = \pm \hat{\mathbf{x}}$. Here $+\hat{\mathbf{x}}$ is the easy driving direction and $-\hat{\mathbf{x}}$ is the hard driving direction. The external drive is increased in small steps of $\delta F^D = 0.001$ and we spend 5×10^5 simulation time steps on each step to evaluate the time averaged velocity measurement, $\langle V_x \rangle = \langle \mathbf{v} \cdot \hat{\mathbf{x}} \rangle$.

3. Easy direction driving

First we consider the case where the external dc drive is applied along the easy or $+x$ direction. In Fig. 2(a) we plot the average skyrmion velocity $\langle V_x \rangle$ as a function of the external drive F^D for several values of the skyrmion density ρ_{sk} in a sample with $\alpha_m/\alpha_d = 0.5$. Figure 2(b) shows $\langle V_x \rangle$ versus ρ_{sk} for selected values of F^D .

In general, for low values of ρ_{sk} the velocity curve $\langle V_x \rangle$ increases linearly with increasing external drive. The flowing skyrmions are widely spaced, as shown in Fig. 3(a), making collective effects almost negligible. The response is similar to that found for a single skyrmion, where a linear dependence of $\langle V_x \rangle$ on F^D is expected. As more skyrmions are added to the sample, the skyrmion-skyrmion interactions become important and the skyrmions begin to compete with each other to pass through the funnel opening. This competition results in a nonlinear $\langle V_x \rangle$ curve, as shown in Fig. 2(a). For each value of F^D there is a critical value of ρ_{sk} above which collective effects appear and the average velocity $\langle V_x \rangle$ begins to drop, as shown in Fig. 2(b). With increasing ρ_{sk} , skyrmions accumulate near the funnel opening, leading to a jamming of the skyrmions and a corresponding reduction in the average velocity.

In Fig. 3 we show some snapshots of the moving skyrmions for the system in Fig. 2. At

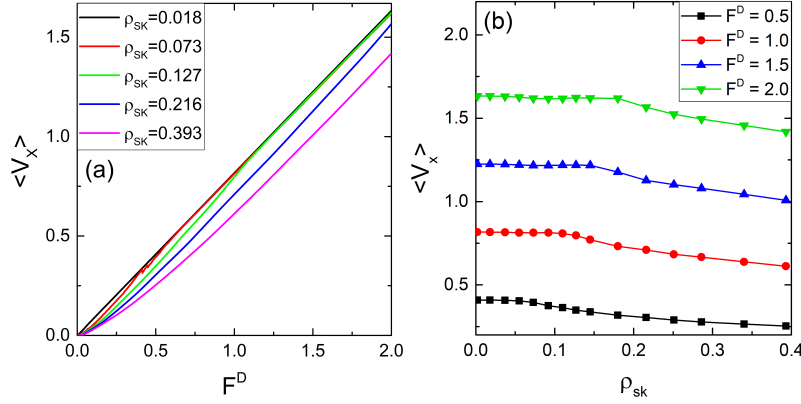


Figure 2. Results for a sample with $\alpha_m/\alpha_d = 0.5$ and easy or $+x$ direction driving. (a) $\langle V_x \rangle$ vs drive amplitude F^D for skyrmion densities $\rho_{sk} = 0.018, 0.073, 0.127, 0.216$, and 0.393 . For high values of F^D , the curves become linear. $\langle V_x \rangle$ decreases with increasing skyrmion density, showing a clear effect of the collective behavior. (b) $\langle V_x \rangle$ vs ρ_{sk} for $F^D = 0.5, 1.0, 1.5$, and 2.0 .

$\rho_{sk} = 0.018$ in Fig. 3(a), the skyrmions interact only weakly and the skyrmion flow is very similar to that found in the single skyrmion limit. For $\rho_{sk} = 0.055$, illustrated in Fig. 3(b), the skyrmions flow in a closely spaced line, increasing the relevance of collective effects. In Fig. 3(c) at $\rho_{sk} = 0.092$, the skyrmions can no longer remain stable in a single line of flow, and competition between skyrmions to pass through the funnel openings begins to appear. For $\rho_{sk} = 0.393$ in Fig. 3(d), multiple skyrmions agglomerate near the funnel opening, decreasing its effective width through their repulsive interactions with approaching skyrmions. This is associated with a significant reduction in the average velocity and can lead to the formation of a *jammed state* of skyrmions near the funnel opening. Here the skyrmions flow almost like a fluid trying to pass through a tight orifice. Due to the Magnus term, when the drive is applied along the $+x$ direction, the skyrmions move at an angle with respect to the drive given by the skyrmion Hall angle, $\theta_{sk}^{\text{int}} = \arctan(\alpha_m/\alpha_d) = -26.56^\circ$, producing a higher concentration of skyrmions in the lower part of the funnel array, as can be seen clearly in Fig. 3(c,d).

4. Hard direction driving

We next apply the drive along the hard or $-x$ direction for a sample with $\alpha_m/\alpha_d = 0.5$. In Fig. 4(a) we show $\langle V_x \rangle$ versus F^D at different skyrmion densities, and in Fig. 4(b) we plot $\langle V_x \rangle$ versus ρ_{sk} for selected values of F^D .

Under hard direction driving, $\langle V_x \rangle = 0$ for all values of F^D when $\rho_{sk} \leq 0.037$, as shown in Fig. 4(b). A snapshot of the skyrmion positions for $\rho_{sk} = 0.018$ and $F^D = 1.5$ appears in Fig. 5(a). Skyrmions are trapped along the vertical walls of the funnel array and are too distant to interact with each other. When $\rho_{sk} > 0.037$, the skyrmions begin to exhibit collective effects and finite motion develops along the hard direction. Interestingly, the magnitude of the average skyrmion velocity, $|\langle V_x \rangle|$, increases as the skyrmion density increases, as illustrated in Fig 4(a). This is different from the behavior of overdamped particles [22, 10], where the average velocity decreases as the particle density increases. In the skyrmion case, the Magnus force is present, and

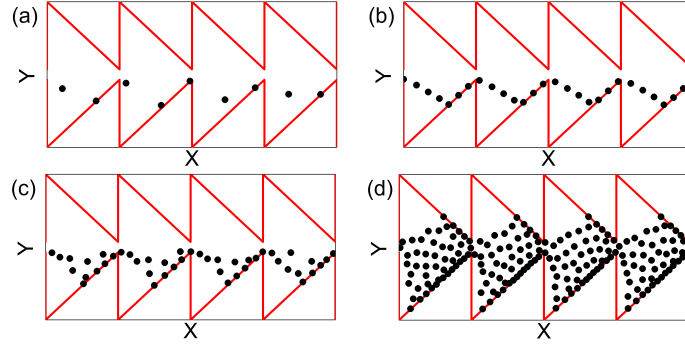


Figure 3. Snapshots of the skyrmion positions for the system in Fig. 2 with $\alpha_m/\alpha_d = 0.5$ and $+x$ driving at $F^D = 1.5$. Red lines are the funnel walls and black dots are skyrmions. The skyrmion density $\rho_{sk} =$ (a) 0.018, (b) 0.055, (c) 0.092 and (d) 0.393. As ρ_{sk} increases, there is a decrease in $\langle V_x \rangle$ due to the competition among skyrmions to pass through the funnel opening. There is also a buildup of skyrmion density in the lower parts of the funnel due to the Magnus effect.

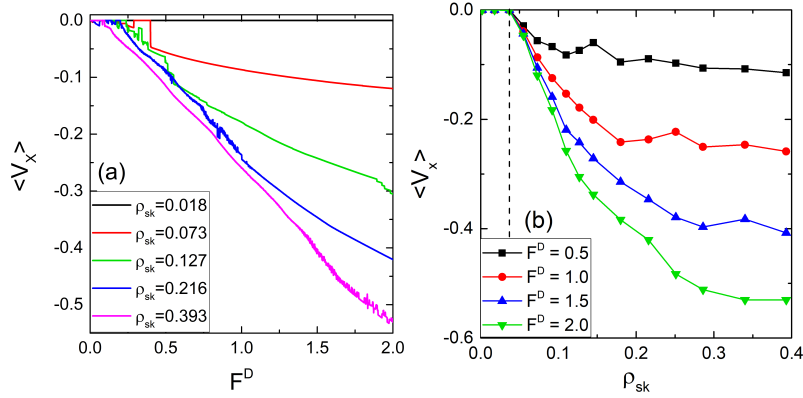


Figure 4. Results for a sample with $\alpha_m/\alpha_d = 0.5$ and hard or $-x$ direction driving. (a) $\langle V_x \rangle$ vs F^D for $\rho_{sk} = 0.018, 0.073, 0.127, 0.216$, and 0.393 . Some of the curves show non-monotonic behavior. (b) $\langle V_x \rangle$ vs ρ_{sk} for $F^D = 0.5, 1.0, 1.5$, and 2.0 , where we find a critical density value (vertical dashed line) of $\rho_{sk}^{\text{crit}} = 0.037$.

it is well-known that gyroscopic effects can significantly influence the skyrmion organization [50]. We believe the phenomenon here is analogous, and that as the density of skyrmions increases, the gyroscopic term favors an easier flow of skyrmions. We also find reentrant pinned phases (RPPs) for all systems with $\rho_{sk} > 0.037$, as shown in Fig. 6. Note that the size and number of RPPs vary with the skyrmion density. For high skyrmion densities, such as $\rho_{sk} = 0.393$, the RPPs are very narrow. On the other hand, for low densities such as $\rho_{sk} = 0.073$, there is only one RPP and it extends over a fairly wide range of F^D . For intermediate skyrmion densities, such as $\rho_{sk} = 0.127$, the RPPs are numerous but are less stable than those found at lower densities.

In Fig. 7 we plot the skyrmion trajectories for the system from Fig. 4(a) and Fig. 6 with

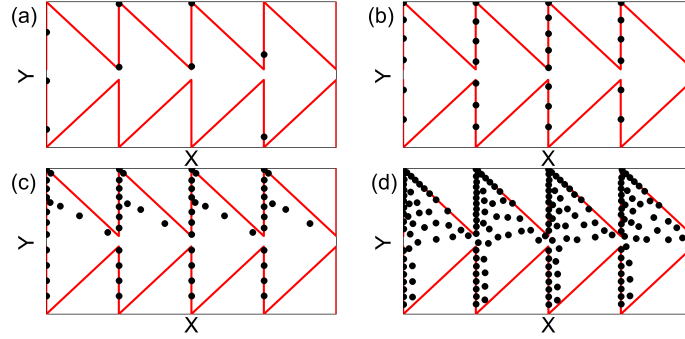


Figure 5. Snapshots of the skyrmion positions for the system in Fig. 4 with $\alpha_m/\alpha_d = 0.5$ and $-x$ driving at $F^D = 1.5$. Red lines are the funnel walls and black dots are skyrmions. The skyrmion density $\rho_{sk} =$ (a) 0.018, (b) 0.055, (c) 0.127 and (d) 0.393.

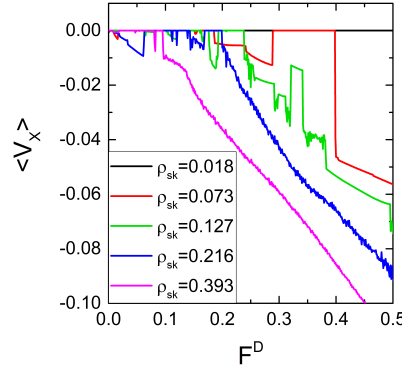


Figure 6. A zoomed in view of the $\langle V_x \rangle$ vs F^D curves from Fig. 4(a) for the system with $\alpha_m/\alpha_d = 0.5$ and $-x$ direction driving over the range $0 < F^D < 0.5$. Reentrant pinning phases appear for all but the smallest value of ρ_{sk} .

$\alpha_m/\alpha_d = 0.5$ at $\rho_{sk} = 0.073$. For $0.185 < F^D < 0.29$, the skyrmions depin and start flowing in the $-x$ direction, as illustrated in Fig. 7(a) for $F^D = 0.26$. In the interval $0.29 < F^D < 0.398$, the skyrmion motion is interrupted by a *clogging effect*, where skyrmions pile up in two of the funnel plaquettes and block the flow, as illustrated in Fig. 7(b) for $F^D = 0.35$. This leads to a zero velocity regime where the skyrmions are trapped. For $F^D > 0.398$, a second depinning transition occurs and the skyrmions start to flow again, as shown in Fig. 7(c) for $F^D = 0.4$.

In Fig. 5 we show some snapshots of the skyrmion positions for the system from Fig. 4. As the skyrmion density increases, skyrmions accumulate along the vertical walls of the funnel array, as illustrated in Fig. 5(a,b). Moreover, due to the finite skyrmion Hall angle, skyrmions tend to accumulate in the upper part of the funnels, as shown in Fig. 5(c,d). The hard direction flow of skyrmions occurs through two types of motion. At low densities, a skyrmion arriving at the upper portion of the vertical wall displaces the skyrmions already stuck along the wall and pushes one of them into the orifice, allowing it to flow into the next plaquette where the process is repeated.

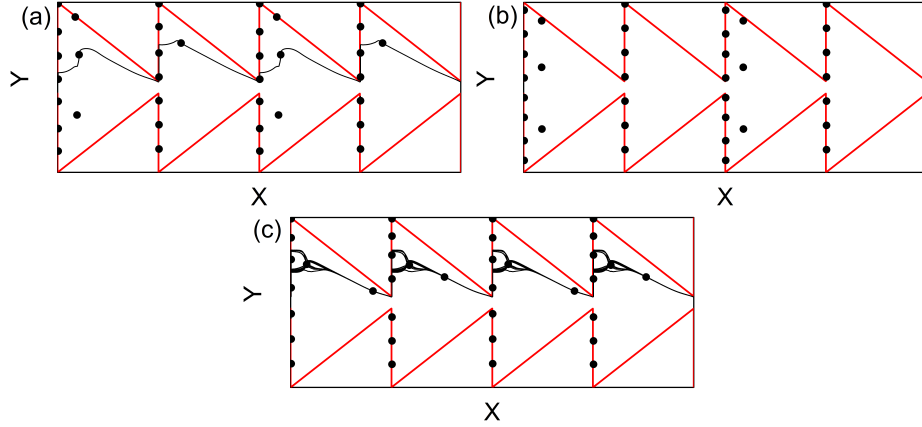


Figure 7. Skyrmion trajectories for the system in Fig. 4 with $-x$ driving and $\alpha_m/\alpha_d = 0.5$ at $\rho_{sk} = 0.073$. Red lines are the funnel walls, black dots are skyrmions, and black lines are the skyrmion trajectories. (a) For $F^D = 0.26$, some of the skyrmions flow through the funnel openings, resulting in finite values of $\langle V_x \rangle$. (b) The reentrant pinned or clogged phase at $F^D = 0.35$, where skyrmions accumulate behind a blockage caused when other skyrmions become trapped on the vertical funnel wall, decreasing the effective width of the funnel opening through their repulsive interactions. (c) The sliding phase at $F^D = 0.4$, where skyrmions are able to flow through the funnel opening again.

For higher densities, the accumulation of skyrmions in the upper portion of each funnel confines the skyrmion motion to a channel along the center line of the funnel, and the wall displacement mechanism is disrupted. Meanwhile, some skyrmions remain permanently trapped in the lower part of the funnel.

4.1. Skyrmion Diode Effect

The difference in the velocity response for driving in the easy and hard directions can be viewed as an example of a skyrmion diode. In diodes, the threshold for transport is different for one direction of drive compared to the other, and the diode effect can be used to create a variety of logic devices [51, 52]. A number of skyrmion diode devices have been proposed using voltage controlled potential barriers [53], asymmetric substrates [54], and even the asymmetry of the motion from the Hall effect [55]. In our system, the diode effect arises because the skyrmions are more susceptible to clogging for hard direction driving than for easy direction driving. To illustrate the diode effect more clearly, in Fig. 8(a) we plot $|V_x|$ versus F_D for driving in the $+x$ and $-x$ directions for the system from Figs. 2 and 4 with $\alpha_m/\alpha_d = 0.5$ at $\rho_{sk} = 0.127$. There is a smooth increase in the velocity-force curve and a depinning force of $F_c = 0$ for $+x$ driving, while for $-x$ driving, the depinning force is finite and has a value near $F_c = 0.25$, as shown in the zoomed in plot of Fig. 8(b). For driving in the hard direction, a clogged regime appears for $0.25 < F_D < 0.5$. When $F_D > 0.5$, the velocity is always higher for $+x$ driving than for $-x$ driving since all of the skyrmions are in motion under easy direction driving, but a portion of the skyrmions become trapped in the funnel corners for hard direction driving. Figure 8 indicates that the velocity-force curves for $+x$ driving remain nonlinear due to the collective effects of the skyrmions moving near the funnel tip. Within our

particle-based model, skyrmions that become trapped at the funnel edges for hard direction driving remain trapped even if the driving force is increased; however, for a real system or in a continuum model, these skyrmions could eventually become strongly distorted and depin for sufficiently large drives.

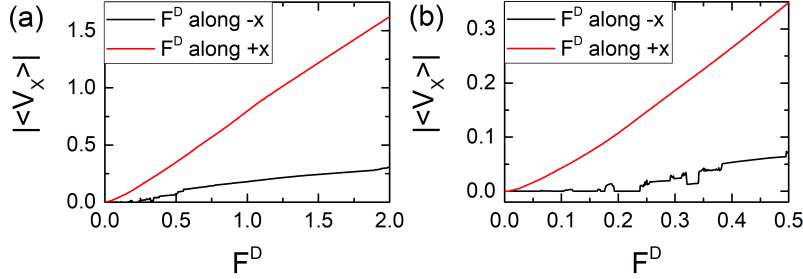


Figure 8. (a) $\langle V_x \rangle$ vs F_D for the system from Figs. 2 and 4 with $\alpha_m/\alpha_d = 0.5$ and $\rho_{sk} = 0.127$ for driving in the $+x$ (red) and $-x$ (black) directions. (b) A zoomed in version of the same plot. There is a skyrmion diode effect in which the critical depinning force is finite only for $-x$ driving, while the velocity response is much higher for $+x$ driving.

5. Effect of varying α_m/α_d for easy direction driving

As shown in previous sections, the Magnus force plays a major role in determining the dynamics of the skyrmions confined to the funnel array. We next vary the ratio α_m/α_d to change the relative importance of the Magnus term in a system with fixed $\rho_{sk} = 0.127$.

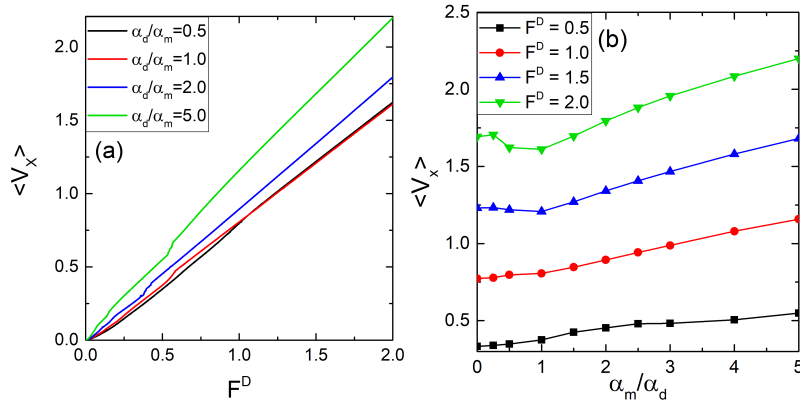


Figure 9. Results for a sample with $\rho_{sk} = 0.127$ under $+x$ driving. (a) $\langle V_x \rangle$ vs F^D for $\alpha_m/\alpha_d = 0.5, 1.0, 2.0$, and 5.0 . (b) $\langle V_x \rangle$ vs α_m/α_d for $F^D = 0.5, 1.0, 1.5$, and 2.0 .

In Fig. 9(a), the plots of $\langle V_x \rangle$ versus F^D for samples with $\rho_{sk} = 0.127$ and varied α_m/α_d under $+x$ driving indicate that the Magnus term modifies the average skyrmion velocity. For stronger Magnus forces of $\alpha_m/\alpha_d > 1.0$, the $\langle V_x \rangle$ versus α_m/α_d curves in Fig. 9(b) show that $\langle V_x \rangle$ always

increases as the Magnus force is increased. When $\alpha_m/\alpha_d \leq 1.0$, however, the behavior changes. In the high drive regime, such as at $F^D = 2.0$, $\langle V_x \rangle$ is nonlinear and non-monotonic over the interval $0 < \alpha_m/\alpha_d < 1.0$. In contrast, for low and intermediate drive regimes, $\langle V_x \rangle$ increases monotonically with increasing Magnus force.

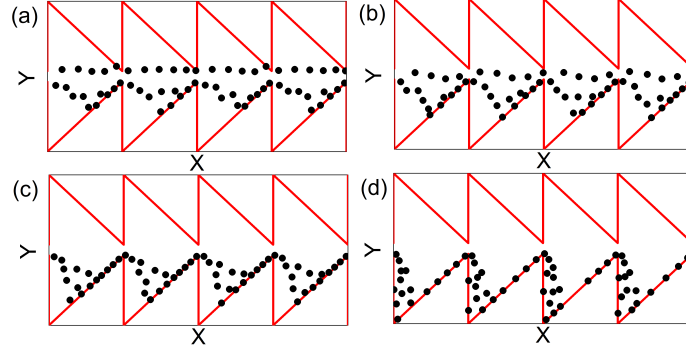


Figure 10. Snapshots of the skyrmion positions for the system in Fig. 5 with $\rho_{sk} = 0.127$ at $F^D = 1.5$. Red lines are the funnel walls and black dots are skyrmions. The Magnus force ratio is $\alpha_m/\alpha_d =$ (a) 0.25, (b) 0.5, (c) 1.0 and (d) 5.0.

In Fig. 10 we show some representative snapshots of the skyrmion positions for the system from Fig. 9 at $F^D = 1.5$. For $\alpha_m/\alpha_d = 0.25$ in Fig. 10(a), where the Magnus force is low, the intrinsic skyrmion Hall angle is $\theta_{sk}^{\text{int}} = -14.04^\circ$ and the skyrmions move along two channels. In the lower channel, the skyrmions follow the direction of the intrinsic skyrmion Hall angle until they strike the diagonal funnel wall, which guides them to the funnel opening. In the upper channel, the skyrmions flow nearly parallel to the drive because the intrinsic skyrmion Hall angle is canceled by the repulsive interactions with skyrmions in the lower channel. As both channels approach the funnel opening, the skyrmions compete to move into the next funnel plaquette. In Fig. 10(b) for $\alpha_m/\alpha_d = 0.5$, the intrinsic Hall angle is higher ($\theta_{sk}^{\text{int}} = -26.56^\circ$) and therefore the skyrmions in the lower channel strike the edge of the diagonal funnel wall further to the left. When $\alpha_m/\alpha_d = 1.0$, as shown in Fig. 10(c), $\theta_{sk}^{\text{int}} = -45^\circ$ and the skyrmion channels begin to merge before reaching the funnel opening, producing a denser single channel. In Fig. 10(d), where $\alpha_m/\alpha_d = 5.0$ and $\theta_{sk}^{\text{int}} = -78.7^\circ$, there are no longer clearly separated channels and the skyrmions flow in a single chaotic band of motion. The presence of two channels of flow for lower Magnus forces facilitates clogging of the skyrmions since the channels compete as they approach the funnel opening, while the single channel or band of flow at higher Magnus forces has no competition and can pass more easily from one funnel plaquette to the next, increasing the average skyrmion velocity.

In Fig. 10(d) we find that the skyrmions along the diagonal funnel wall are more widely spaced than the other skyrmions. This is caused by the velocity boost that the skyrmions receive when they are flowing against the wall. Figure 11 describes the origin of the velocity boost effect schematically. In Fig. 11(a) we highlight a single funnel where the high speed flow along the funnel wall occurs, with one skyrmion circled. The forces on this skyrmion are illustrated in Fig. 11(b). The driving force \mathbf{F}_D is in the $+x$ direction, and the repulsive force from the wall F_{wall} acts perpendicular to the wall. The vector sum of these two forces is \mathbf{F}_R . According to equation (1), the Magnus force rotates \mathbf{F}_R clockwise by an amount θ_{sk}^{int} , toward the direction of \mathbf{v} . Depending on the particular value of

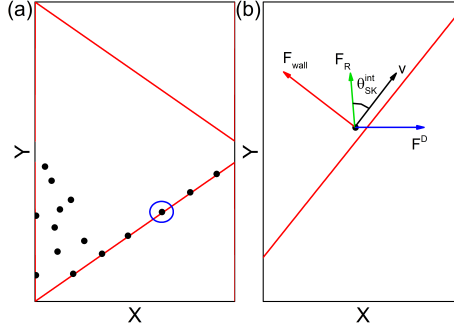


Figure 11. (a) A zoomed in image of a single funnel from Fig. 10(d). Red lines are the funnel walls and black dots are skyrmions. We focus on the circled skyrmion. (b) Force diagram indicating the force components that contribute to the velocity boost experienced by a skyrmion in the direction parallel to the funnel wall. \mathbf{F}_D (blue) is the driving force in the $+x$ direction. \mathbf{F}_{wall} (red) is the repulsive force from the funnel wall, which acts perpendicular to the wall. \mathbf{F}_R (green) is the sum of \mathbf{F}_D and \mathbf{F}_R . The Magnus force rotates \mathbf{F}_R clockwise by an amount $\theta_{sk}^{\text{int}} = \arctan(\alpha_m/\alpha_d)$. In the illustrated case, this angle exactly matches the angle of the funnel wall, and the entire force \mathbf{F}_R acts in the direction of the skyrmion velocity \mathbf{v} (black) along the funnel wall, giving a maximal velocity boost effect. In more general cases, the skyrmion Hall angle and funnel wall angles are different, and only a portion of \mathbf{F}_R contributes to the boost effect.

α_m/α_d , this will bring a greater or lesser portion of \mathbf{F}_R into alignment with the skyrmion velocity \mathbf{v} parallel to the funnel wall, producing a velocity boost. In the illustrated case, θ_{sk}^{int} matches the angle of the funnel wall exactly and the velocity boost effect is maximized.

6. Effect of varying α_m/α_d for hard direction driving

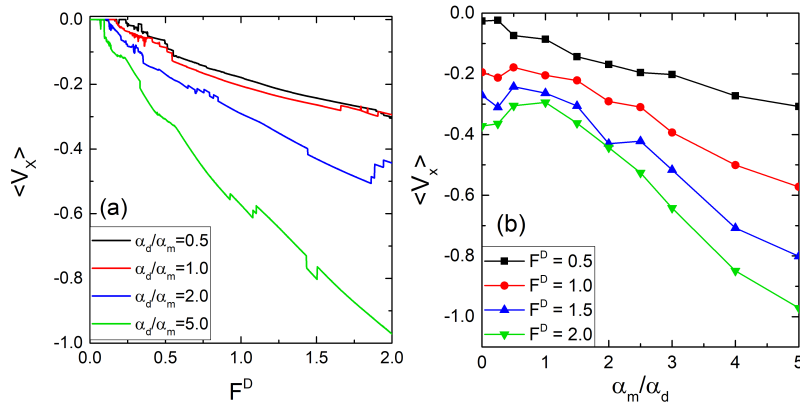


Figure 12. Results for a sample with $\rho_{sk} = 0.127$ under $-x$ driving. (a) $\langle V_x \rangle$ vs F^D for $\alpha_m/\alpha_d = 0.5, 1.0, 2.0$, and 5.0 . (b) $\langle V_x \rangle$ vs α_m/α_d for $F^D = 0.5, 1.0, 1.5$, and 2.0 .

We now apply the drive along the hard or $-x$ direction while varying α_m/α_d for samples with $\rho_{sk} = 0.127$. In Fig. 12(a), we plot $\langle V_x \rangle$ versus F^D for different values of α_m/α_d . There is an overall increase in the magnitude of the average skyrmion velocity as the Magnus term becomes larger, which is more clearly illustrated in the plot of $\langle V_x \rangle$ versus α_m/α_d for selected values of F^D in Fig. 12(b). Note that reentrant pinning phases (RPPs) are also affected by the Magnus intensity. The RPPs are more prominent for low values of α_m/α_d but the clogging effect is diminished as the Magnus term becomes stronger.

Figure 12(a) shows that the depinning threshold changes as α_m/α_d is varied. For higher values of α_m/α_d , the depinning threshold shifts to lower values of F^D . In Fig. 12(b), $\langle V_x \rangle$ has a nonlinear and non-monotonic dependence on α_m/α_d for intermediate and high drives. This is similar to the results found for $+x$ driving in Fig. 9.

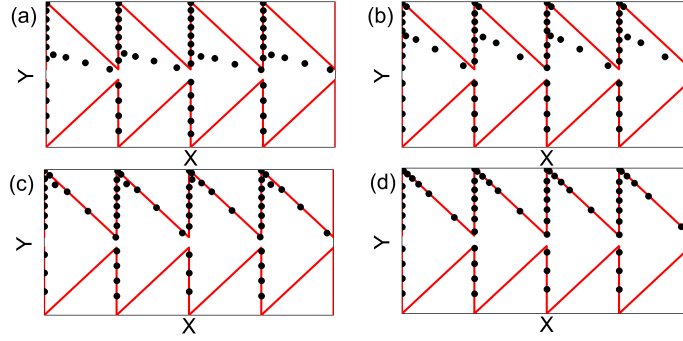


Figure 13. Snapshots of the skyrmion positions for the system in Fig. 12 with $\rho_{sk} = 0.127$ at $F^D = 1.5$. Red lines are the funnel walls and black dots are skyrmions. The Magnus force ratio is $\alpha_m/\alpha_d =$ (a) 0.25, (b) 0.5, (c) 1.0 and (d) 5.0.

In Fig. 13(a) we illustrate snapshots of the skyrmion positions for the system in Fig. 12 at $F^D = 1.5$. For low values of α_m/α_d , the intrinsic skyrmion Hall angle is reduced and as a consequence more skyrmions remain trapped in the funnel plaquettes. For example, in Fig. 13(a) at $\alpha_m/\alpha_d = 0.25$, the channel of flowing skyrmions strikes the vertical funnel wall just above the point where the bottom skyrmion is trapped by the wall, releasing that skyrmion and allowing it to pass into the next funnel plaquette; however, all of the other skyrmions higher up on the funnel wall remain trapped permanently. Since relatively few skyrmions are able to move, the average skyrmion velocity is reduced. For $\alpha_m/\alpha_d = 0.5$, shown in Fig. 13(b), the skyrmion channel strikes the vertical funnel wall approximately at its center, pushing a larger number of skyrmions toward the funnel opening and reducing the number of skyrmions that are permanently pinned. In Figs. 13(c,d) for $\alpha_m/\alpha_d = 1.0$ and 5.0 , respectively, the moving skyrmion channel pushes almost all of the skyrmions along the vertical funnel wall toward the funnel opening, leading to a much higher average skyrmion velocity. In addition, according to the mechanism explained in Fig. 11, the skyrmion velocity for sliding along the diagonal funnel walls can be boosted considerably. The channel motion of skyrmions boosted by the Magnus effect also reduces the depinning threshold, as shown in Fig. 12(a).

7. Clogging Dynamics

In systems that exhibit clogging, such as flow through apertures or bottlenecks, the flow is typically probabilistic in nature, and the particles may flow for some period of time before reaching a clogged configuration [13, 14, 15, 16, 17]. In contrast, systems that exhibit jamming have a unique density above which the flow ceases [56, 57]. In our system, the initial skyrmion configurations are obtained using simulated annealing. If somewhat different initial conditions are used, the clogging behavior found for $-x$ driving remains robust but the specific drives at which velocity dips or reentrant pinning occur can shift to slightly different locations for different realizations. For driving in the easy direction, however, the velocity curves remain unchanged for different initial configurations.

In Fig. 14(a) we plot $\langle V_x \rangle$ versus F^D for driving in the hard direction in a system with $\rho_{sk} = 0.073$ and $\alpha_m/\alpha_d = 0.5$ for five different realizations of the initial conditions. For $F^D > 0.45$, the curves are smooth and are insensitive to the initial conditions, while for $F^D < 0.45$, there are some differences in the location of jumps and drops in the velocity for different realizations; however, all of the realizations have jumps for $F^D < 0.45$, indicating that there is a well defined clogging regime. In Fig. 14(b), we plot a dynamic phase diagram as a function of F^D versus ρ_{sk} showing how the clogging regime evolves. As the skyrmion density increases, the windows of drive over which clogging can occur are reduced. In general, we find that there is a region in which some flow occurs before a clogged state is established. In clogging systems, the probability to clog also depends on the rate of flow through the aperture, such that for lower flow rates the particles can generally flow, while at higher flow rates clogging becomes more likely. In the skyrmion system, at high F^D the drive can break up the clogs. The boundaries in Fig. 14(b) are obtained using individual realizations at each point. For multiple realizations at each point, the system would be better described as showing clogging behavior below the red solid line and flowing behavior above the red solid line.

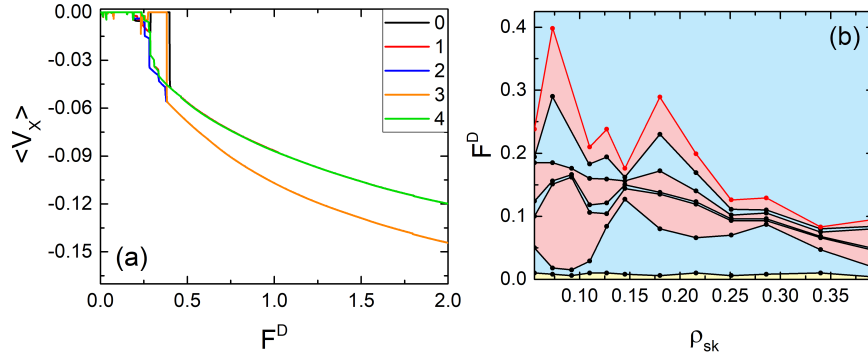


Figure 14. (a) Results for a sample with $\rho_{sk} = 0.127$ under $-x$ driving at $\alpha_m/\alpha_d = 0.5$ for five different realizations of the initial conditions. The clogging events occur at slightly different drives, while for $F^D > 0.45$, the system exhibits continuous flow that is not sensitive to the initial conditions. (b) Dynamic phase diagram as a function of F^D vs ρ_{sk} showing pinned (yellow), clogged (red), and flowing (blue) states for the system in panel (a). Below the red solid line, the system shows clogging behavior, while above the red solid line, the flow is continuous.

8. Discussion

In our system we consider a particle-based model in which the number of particles is fixed and cannot change. For real skyrmion systems, it is possible for skyrmions to be created or annihilated due to interactions with the current and with barriers. Additionally, skyrmions could change shape when interacting with structures or with the drive. An interesting future direction would be to consider continuum-based models for skyrmions and the skyrmion-barrier interactions [35, 58, 59] where the shape of the skyrmion could change as it moves through the funnel constrictions. In the clogging phase, the skyrmions could also become compressed or change shape, and it would be interesting to explore whether such extra degrees of freedom would enhance or decrease the clogging effects. The effect of temperature could also be important, since in some cases skyrmions are known to exhibit Brownian like motion [60]. In this case, thermal effects on the transport curves for driving in the easy direction would be small; however, in the clogging regime, thermal effects could have a strong impact by causing unclogging events, or allowing the velocity at a fixed drive to undergo thermally induced jumps from clogged to unclogged states. We have focused on ferromagnetic skyrmions; however, different effects could arise for driving other kinds of skyrmion textures such as antiferromagnetic skyrmions, merons, or elliptical skyrmions [61]. There are various methods that could be used to create funnel structures experimentally, such as etched samples with thickness modulations, the addition of adatoms in certain patterns on the surface [62], or ion irradiation [63].

9. Summary

Using a particle based model we simulated the collective effects of skyrmions interacting with a linear array of funnel potentials at zero temperature for external dc driving applied along the easy or hard direction. For easy direction driving, we find that at low skyrmion densities the dynamics is very similar to that observed in the single skyrmion limit, with the average velocity increasing linearly with increasing drive. As the skyrmion density increases, collective effects become relevant, and for high skyrmion densities the skyrmions may jam near the funnel opening, obstructing the flow. For hard direction driving, skyrmion motion occurs only above a critical skyrmion density $\rho_{sk}^{\text{crit}} = 0.037$, where the interskyrmion distance becomes small enough for collective effects to emerge. For densities above the critical value, the skyrmions flow in a window of driving forces before entering a reentrant pinning phase (RPP) where the skyrmion motion is interrupted due to a pile up of skyrmions inside funnel plaquettes, leading to the formation of a clogged state. Skyrmion motion in the clogged state drops to zero until the drive is increased above a second depinning threshold, where the blockage is destroyed and the skyrmions can flow through the funnels again. We also observe a skyrmion diode effect in which there is a finite critical depinning threshold for hard direction driving but a zero critical threshold for easy direction driving. The velocity for hard direction driving is always lower than that found for easy direction driving.

In addition to studying the effect of changing the skyrmion density, we also analyze the effects of modifying the relative importance of the Magnus term by varying the ratio α_m/α_d . For both directions of applied drive, the skyrmion velocity has a nonlinear and non-monotonic dependence on α_m/α_d . Moreover, the Magnus term also determines the spatial distribution of the skyrmions inside the funnels, since the skyrmion Hall angle causes skyrmions to be displaced toward the lower half of the funnel for easy direction driving and toward the upper half of the funnel for hard direction driving. Increasing the strength of the Magnus term changes the RPPs found for hard direction driving by making it more difficult for a clogged state of skyrmions to form.

Acknowledgments

This work was supported by the US Department of Energy through the Los Alamos National Laboratory. Los Alamos National Laboratory is operated by Triad National Security, LLC, for the National Nuclear Security Administration of the U. S. Department of Energy (Contract No. 892333218NCA000001).

J.C.B.S and N.P.V acknowledges funding from Fundação de Amparo à Pesquisa do Estado de São Paulo - FAPESP (Grants 2021/04941-0 and 2017/20976-3 respectively).

References

- [1] Köppl M, Henseler P, Erbe A, Nielaba P and Leiderer P 2006 *Physical Review Letters* **97** 208302
- [2] Dobrovolskiy O V, Begun E, Huth M and Shklovskij V A 2012 *New Journal of Physics* **14** 113027
- [3] Barrozo P, Moreira A A, Aguiar J A and Andrade J S 2009 *Physical Review B* **80** 104513
- [4] Piacente G and Peeters F M 2005 *Physical Review B* **72** 205208
- [5] Yu K, Hesselberth M B S, Kes P H and Plourde B L T 2010 *Physical Review B* **81** 184503
- [6] Rees D G, Totsuji H and Kono K 2012 *Physical Review Letters* **108** 176801
- [7] Zimmermann U, Smallenburg F and Löwen H 2016 *Journal of Physics: Condensed Matter* **28** 244019
- [8] Wambaugh J F, Reichhardt C, Olson C J, Marchesoni F and Nori F 1999 *Physical Review Letters* **83** 5106–5109
- [9] Yu K, Heitmann T W, Song C, DeFeo M P, Plourde B L T, Hesselberth M B S and Kes P H 2007 *Physical Review B* **76** 220507
- [10] Reichhardt C J O and Reichhardt C 2010 *Physical Review B* **81** 224516
- [11] Vlasko-Vlasov V, Benseman T, Welp U and Kwok W K 2013 *Superconductor Science and Technology* **26** 075023
- [12] Karapetrov G, Yefremenko V, Mihajlović G, Pearson J E, Iavarone M, Novosad V and Bader S D 2012 *Physical Review B* **86** 054524
- [13] Redner S and Datta S 2000 *Physical Review Letters* **84** 6018–6021
- [14] Zuriguel I, Parisi D R, Hidalgo R C, Lozano C, Janda A, Gago P A, Peralta J P, Ferrer L M, Pugnali L A, Clément E, Maza D, Pagonabarraga I and Garcimartín A 2014 *Scientific Reports* **4** 7324
- [15] To K, Lai P Y and Pak H K 2001 *Physical Review Letters* **86** 71–74
- [16] Helbing D, Farkas I and Vicsek T 2000 *Nature* **407** 487–490
- [17] Nguyen H T, Reichhardt C and Reichhardt C J O 2017 *Physical Review E* **95** 030902
- [18] Reichhardt C and Olson Reichhardt C J 2010 *Physica C: Superconductivity* **470** 722–725
- [19] Olson Reichhardt C J and Reichhardt C 2013 *Journal of Superconductivity and Novel Magnetism* **26** 2005–2008
- [20] Villegas J E, Gonzalez E M, Gonzalez M P, Anguita J V and Vicent J L 2005 *Physical Review B* **71** 024519
- [21] Villegas J E, Savel'ev S, Nori F, Gonzalez E M, Anguita J V, García R and Vicent J L 2003 *Science* **302** 1188–1191
- [22] Reichhardt C J O and Reichhardt C 2018 *Journal of Physics: Condensed Matter* **30** 244005
- [23] Martinez R, Alarcon F, Luis Aragonés J and Valeriani C 2020 *Soft Matter* **16** 4739–4745
- [24] Wan M B, Olson Reichhardt C J, Nussinov Z and Reichhardt C 2008 *Physical Review Letters* **101** 018102
- [25] Berdakin I, Jeyaram Y, Moshchalkov V V, Venken L, Dierckx S, Vanderleyden S J, Silhanek A V, Condat C A and Marconi V I 2013 *Physical Review E* **87** 052702
- [26] Migita K, Yamada K and Nakatani Y 2020 *Appl. Phys. Express* **13** 073003
- [27] Souza J C B, Vizir N P, Reichhardt C J O, Reichhardt C and Venegas P A 2021 *Physical Review B* **104** 054434
- [28] Mühlbauer S, Binz B, Jonietz F, Pfleiderer C, Rosch A, Neubauer A, Georgii R and Böni P 2009 *Science* **323** 915–919
- [29] Fert A, Reyren N and Cros V 2017 *Nature Reviews Materials* **2** 1–15
- [30] Fert A, Cros V and Sampaio J 2013 *Nature Nanotechnology* **8** 152–156
- [31] Jonietz F, Mühlbauer S, Pfleiderer C, Neubauer A, Münzer W, Bauer A, Adams T, Georgii R, Böni P, Duine R A, Everschor K, Garst M and Rosch A 2010 *Science* **330** 1648–1651
- [32] Schulz T, Ritz R, Bauer A, Halder M, Wagner M, Franz C, Pfleiderer C, Everschor K, Garst M and Rosch A 2012 *Nature Physics* **8** 301–304
- [33] Yu X Z, Kanazawa N, Zhang W Z, Nagai T, Hara T, Kimoto K, Matsui Y, Onose Y and Tokura Y 2012 *Nature Communications* **3**
- [34] Nagaosa N and Tokura Y 2013 *Nature Nanotechnology* **8** 899–911
- [35] Iwasaki J, Mochizuki M and Nagaosa N 2013 *Nature Communications* **4** 1463

- [36] Jiang W, Zhang X, Yu G, Zhang W, Wang X, Benjamin Jungfleisch M, Pearson J E, Cheng X, Heinonen O, Wang K L, Zhou Y, Hoffmann A and te Velthuis S G E 2017 *Nature Physics* **13** 162–169
- [37] Litzius K, Lemesch I, Krüger B, Bassirian P, Caretta L, Richter K, Büttner F, Sato K, Tretiakov O A, Förster J, Reeve R M, Weigand M, Bykova I, Stoll H, Schütz G, Beach G S D and Kläui M 2017 *Nature Physics* **13** 170–175
- [38] Reichhardt C, Ray D and Reichhardt C J O 2015 *Physical Review B* **91** 104426
- [39] Vizir N P, Souza J C B, Reichhardt C, Reichhardt C J O and Venegas P A 2021 *Journal of Physics: Condensed Matter* **33** 305801
- [40] Feilhauer J, Saha S, Tobik J, Zelent M, Heyderman L J and Mruczkiewicz M 2020 *Physical Review B* **102** 184425
- [41] Göbel B and Mertig I 2021 *Scientific Reports* **11** 3020
- [42] Vizir N P, Reichhardt C J O, Venegas P A and Reichhardt C 2020 *Journal of Physics Communications* **4** 085001
- [43] Reichhardt C, Ray D and Reichhardt C J O 2015 *New Journal of Physics* **17** 073034
- [44] Ma X, Reichhardt C J O and Reichhardt C 2017 *Physical Review B* **95** 104401
- [45] Vizir N P, Reichhardt C, Venegas P A and Reichhardt C J O 2021 *Journal of Magnetism and Magnetic Materials* **528** 167710
- [46] Reichhardt C and Reichhardt C J O 2016 *New Journal of Physics* **18** 095005
- [47] Montoya S A, Tolley R, Gilbert I, Je S G, Im M Y and Fullerton E E 2018 *Physical Review B* **98** 104432
- [48] Reichhardt C, Ray D and Reichhardt C J O 2018 *Physical Review B* **98** 134418
- [49] Lin S Z, Reichhardt C, Batista C D and Saxena A 2013 *Physical Review B* **87** 214419
- [50] Brown B L, Täuber U C and Pleimling M 2018 *Physical Review B* **97** 020405
- [51] Katz R H and Borriello G 2005 *Contemporary Logic Design* (Pearson Prentice Hall, Upper Saddle River)
- [52] Kitai A 2011 *Principles of Solar Cells, LEDs and Diodes* (Wiley, Chichester)
- [53] Zhao L, Liang X, Xia J, Zhao G and Zhou Y 2020 *Nanoscale* **17** 9507
- [54] Jung D H, Han H S, Kim N, Kim G, Jeong S, Lee S, Kang M, Im M Y and Lee K S 2021 *Phys. Rev. B* **104**(6) L060408
- [55] Feng Y, Zhang X, Zhao G and Xiang G 2022 *IEEE Trans. Electron Devices* **69** 1293
- [56] Stoop R L and Tierno P 2018 *Commun. Phys.* **1** 68
- [57] Peter H, Libál A, Reichhardt C and Reichhardt C J O 2018 *Sci. Rep.* **8** 10252
- [58] Lin S Z, Reichhardt C, Batista C D and Saxena A 2013 *Phys. Rev. B* **87**(21) 214419
- [59] Del-Valle N, Castell-Queralt J, González-Gómez L and Navau C 2022 *APL Mater.* **10** 010702
- [60] Zhao L, Wang Z, Zhang X, Liang X, Xia J, Wu K, Zhou H A, Dong Y, Yu G, Wang K L, Liu X, Zhou Y and Jiang W 2020 *Phys. Rev. Lett.* **125**(2) 027206
- [61] Göbel B, Mertig I and Tretiakov O A 2021 *Phys. Rep.* **895** 1
- [62] Arjana I G, Fernandes I L, Chico J and Lounis S 2020 *Sci. Rep.* **10** 14655
- [63] Juge R, Bairagi K, Rana K G, Vogel J, Sall M, Mailly D, Pham V T, Zhang Q, Sisodia N, Foerster M, Aballe L, Belmeguenai M, Roussigné Y, Auffret S, Buda-Prejbeanu L D, Gaudin G, Ravelosona D and Boulle O 2021 *Nano Lett.* **21**(7) 2989–2996